Langmuir

Article

pubs.acs.org/Langmuir

Multifunctional Magnetic Mesoporous Silica Nanocomposites with Improved Sensing Performance and Effective Removal Ability toward Hg(II)

Yanyan Wang,[†,‡] Bin Li,[*,†] Liming Zhang,[†] Peng Li,[†,‡] Lianlian Wang,[†,‡] and Jin Zhang[†,‡]

[†]State Key Laboratory of Luminescence and Applications, Changchun Institute of Optics Fine Mechanics and Physics, Chinese Academy of Sciences, Changchun 130033, P. R. China

[‡]Graduate School of the Chinese Academy of Sciences, Chinese Academy of Sciences, Beijing 100039, P. R. China

Supporting Information

ABSTRACT: In the present work, a multifunctional inorganic−organic hybrid nanomaterial (MMS−Py) was prepared by the immobilization of a pyrene-based receptor (Py) within the channels of magnetic mesoporous silica nanocomposites (MMS), and characterized by scanning electron microscopy, transmission electron microscopy, Fourier transform infrared spectroscopy, X-ray diffraction, N_2 adsorption/desorption, superconducting quantum interference device, and photoluminescence spectra. This multifunctional nanomaterial exhibits superparamagnetic behavior, ordered mesoporous characteristics, and significantly improved fluorescence sensing properties that allow for highly sensitive and reproducible Hg^{2+} detection. The fluorogenical responses of MMS-Py are stable over a broad pH range. A detection limit of 1.72 ppb is obtained, which is 2 orders of magnitude lower than that based on bulk mesoporous materials. Additionally, this nanomaterial shows high performance in convenient magnetic separability and efficient removal of Hg^{2+}. These results indicate that these multifunctional nanocomposites may find potential applications for simple detection and easy removal of Hg^{2+} in biological, toxicological, and environmental areas.

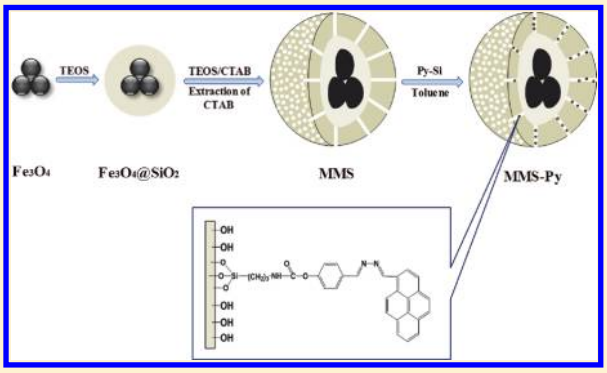

1. INTRODUCTION

Detection and removal of heavy-metal ions, such as Pb^{2+}, Cd^{2+},Cu^{2+}, and Hg^{2+}, have received considerable attention owing to their potential implications in environmental and biological fields.[1] Mercury is one of the most toxic and dangerous heavy-metal elements because of its high affinity for thiol groups in proteins and enzymes, leading to dysfunction of cells and consequently many health problems in brain, kidney, and central nervous system.[2] Therefore, concerns for toxic damage of mercury provide a motivation to explore highly selective and sensitive materials to monitor, absorb, and remove Hg^{2+} from biological and environmental samples.

As an important family of nanocomposites, magnetic nanocomposites with magnetically responsive cores and functional shells have attracted increasing attention because of their attractive physical and chemical properties, such as large surface areas, magnetic properties, low toxicity, and chemically modifiable surfaces that make them attractive for various applications ranging from drug/gene/RNA delivery carriers, multimodal imaging agents, water treatment adsorbents, and catalysts for various reactions.[3−6]

The receptor-immobilized magnetic mesoporous silica nanocomposites are considered to have some important advantages as a solid chemosensor and adsorbent in heterogeneous solid−liquid phases.[7] First, the good optical transparency in visible region and the favorable biocompatibility make receptor-immobilized magnetic mesoporous silica nanocomposites promising for optical sensors. Second, the large surface area and open pore structure provide an amplified target−receptor interface, making them desirable for sensing applications.[8] When served as nanoreactors, analytes are brought nearby sensor probes. The sensing capabilities can thus be enhanced since the unique open mesopore is readily accessible, which accelerates the adsorption and access of guest molecules, leading to an enhanced local concentration and thus a lower detection limit. Furthermore, mesoporous nanostructures can enable a rapid diffusion of analytes across the large surface area, showing a short response time.[9] Third, their low-cost, easy recyclability via external magnetic field and suitable chemical treatments make them convenient to remove pollutants and toxic metal ions from samples. The magnetic property enables the operator to trap the materials at a distinct spot and to guide them to a desired position within the measurement setup.

Received: November 15, 2011
Revised: December 16, 2011
Published: December 20, 2011

Scheme 1. Synthesis Procedure for the Functionalized Material MMS-Py

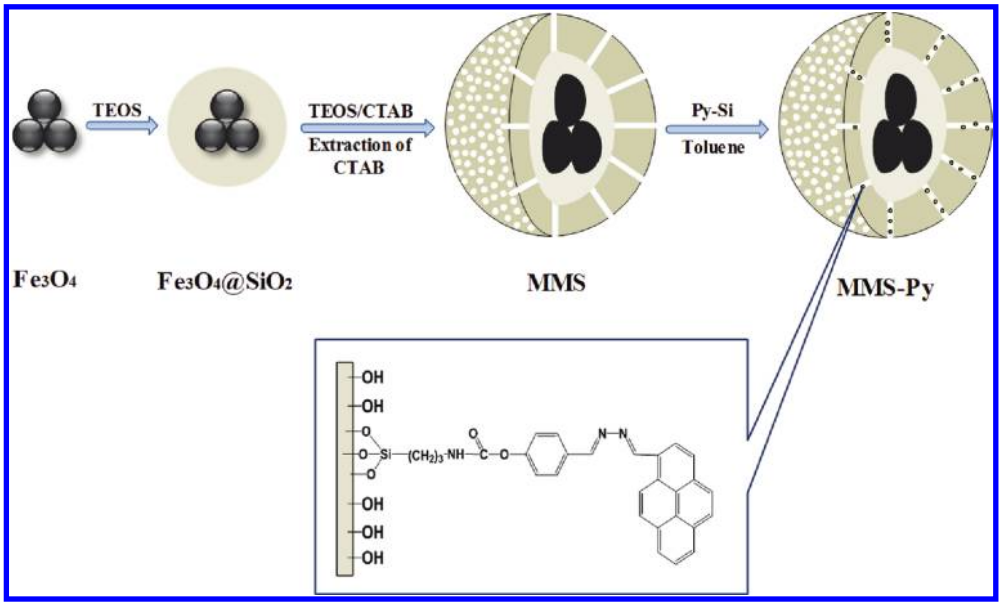

Thereby, the signal intensity is increased, at the same time, optical interferences with the medium are reduced.

Recently, some research groups have reported organic–inorganic hybrid materials for detection and removal of Hg^{2+}.[10] These materials, however, suffer from some drawbacks. For example, the sensing molecule react with mercury ion irreversibly and cannot be recycled and reused. In addition, their sensitivity to operational pH also limits their wide applications. In previous study, our group have reported a pyrene-functionalized SBA-15 silica for Hg^{2+} detection, showing good linearity and regenerative ability.[11] Unfortunately, the unsatisfied detection limit and finite functional components are still waiting to be further improved. It is expected that multifunctional nanomaterials are one of the best choices to overcome above problems because of their improved physical and chemical properties over single-component counterparts.

Herein, we report an inorganic–organic hybrid nanomaterial by immobilizing pyrene-based receptor Py onto the inner surface of magnetic mesoporous silica nanocomposite (MMS) as a convenient approach for highly selective/sensitive detection and further separation of Hg^{2+}. The well-designed nanomaterials show high performance in detection of Hg^{2+} with a detection limit as low as 1.72 ppb, and the fluorogenical responses are reversible and reliable within a wide pH range. Furthermore, MMS-Py can quickly separate Hg^{2+} from the solution with external magnetic field, and possesses good reusability.

2. EXPERIMENTAL DETAILS

2.1. Materials. Tetraethoxysilane (TEOS, Tianjin Chemicals Co.), 3-(triethoxysilyl)-propyl isocyanate (TESPIC, Aldrich), 4-hydroxybenzaldehyde (Aldrich) and 1-pyrenecarboxaldehyde (Aldrich) were used as received. Cetyltrimethylammonium bromide (CTAB), sodium dodecyl sulfate (SDS), ferric trichloride, anhydrous sodium acetate, ammonia solution (28 wt %), hydrazine hydrate (85%), and ethylene glycol were purchased from Shanghai Chemical Company (Shanghai, China). Mercury nitrate and the other inorganic metal salts were purchased from Shanghai Chemical Company (Shanghai, China). The solvent toluene and tetrahydrofuran were used after desiccation with anhydrous sodium sulfate (Shanghai, China). Concentrated HCl was obtained from Shanghai Chemical Company (Shanghai, China). Analytical grade solvents and compounds were used without further purifications for preparation.

2.2. Synthesis of Magnetic Mesoporous Sillia Nanocomposites (MMS). The spherical magnetic particles were prepared through a solvothermal reaction according to the literature.[12] Then, the MMS were synthesized as follows: Fe_3O_4 nanoparticles (0.05 g) were treated with ethanol (20 mL) under ultrasonication for 30 min. Then the magnetite particles were well dispersed in a mixture of ethanol (20 mL), deionized water (10 mL), and concentrated ammonia solution (0.5 mL, 28 wt %). Then TEOS (0.03 g) was added dropwise to the solution. After being mechanically stirred for 6 h at room temperature, the products were separated, and then redispered in a mixed solution containing of CTAB (0.15 g), deionized water (40 mL), concentrated ammonia solution (0.60 mL, 28 wt %) and ethanol (30 mL). The resulting solution was stirred for 30 min. TEOS (0.40 g) was added dropwise to the solution with vigorous stirring. After reaction for 6 h, the product was centrifuged, washed repeated with ethanol and distilled water, and then dried in vacuum at 80 °C overnight. The above coating process was repeated twice. Finally, the CTAB templating agents were removed using an acid extraction process: the synthesized core–shell nanoparticles (0.1 g) were suspended in ethanol (100 mL) and concentrated HCl (2 M, 5 mL). The suspension was vigorously stirred for 48 h, and the products were then collected via filtration, washed with ethanol and distilled water in sequence, and dried under vacuum at 80 °C for 24 h. FT-IR analysis (see Supporting Information, Figure S1) shows the as-synthesized MMS and surfactant-extracted MMS, indicating that the templates were successfully removed. The extraction was repeated for three times.

2.3. Synthesis of Pyrene-Functionalized Magnetic Mesoporous Sillia Nanocomposites (MMS–Py). Pyrene-based receptor Py was easily prepared by treating 1-(4′-hydroxyphenyl)-4-pyrenyl-2,3-diaza-1,3-butadiene (Py–OH) with TESPIC according to our previous reported procedure.[11] Then Py-Si (1.00 g) and MMS (1.00 g) were suspended in anhydrous toluene (50 mL) and stirred under reflux in N_2 atmosphere for 48 h. Then, the precipitate was filtered, and adequately washed several times with toluene and THF to rinse away any surplus Py. The final product was produced in 0.50 g yield and denoted as MMS–Py.

2.4. Characterization. Transmission electron microscopy (TEM) images were taken with a JEM-2010 transmission election microscope made by Japanese JEOL Company. Scanning electronic microscopy (SEM) images were recorded on a Hitachi S-4800 microscope. The samples were dispersed in the mixture of ethanol and collodion (*V*/*V*

dx.doi.org/10.1021/la204494v | *Langmuir* 2012, 28, 1657–1662

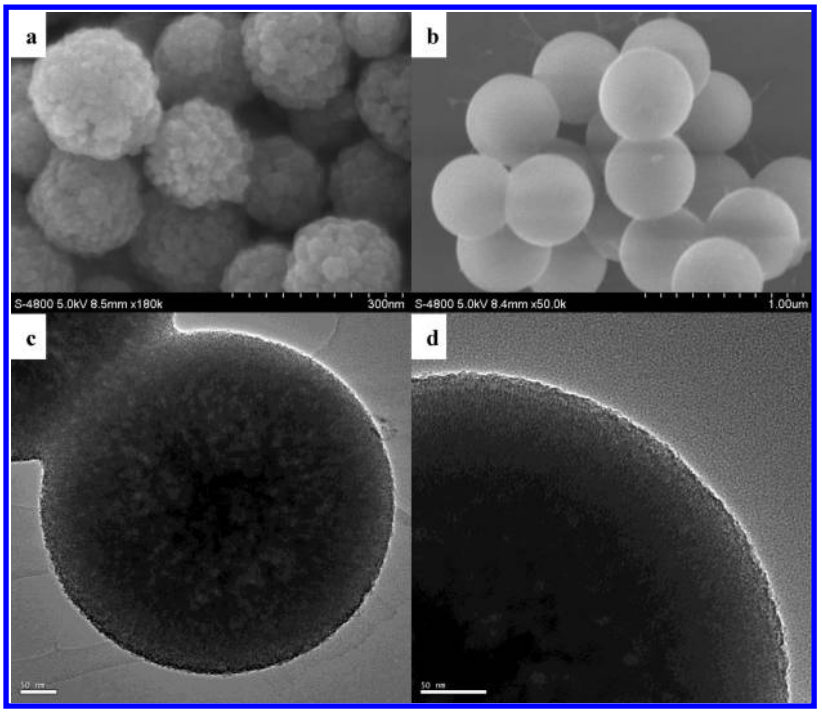

Figure 1. SEM images of the Fe_3O_4 particles before (a) and after (b) the silica coating, TEM images of MMS microspheres (c) and its magnified view (d).

= 8:1) and then collected using silicon wafer before measurements. Fourier-transform infrared (FT-IR) spectra were collected on a Nicolet Fourier spectrophotometer using KBr pellets. Powder X-ray diffraction (XRD) patterns were recorded on a Bruker D4 X-ray diffractometer (Germany) with Ni-filtered Cu K radiation (40 kV, 40 mA). The nitrogen adsorption and desorption isotherms were measured at 77 K by using a Nova l000 analyzer. Before measurements, the samples were degassed in a vacuum at 373 K for 4 h. Surface areas were calculated by the Brunauer–Emmett–Teller (BET) method, and the pore volume and pore size distributions were calculated using the Barrett–Joyner–Halenda (BJH) model. Magnetization measurements were performed on a MPMS-XL-5 superconducting quantum interference device (SQUID) magnetometer at 300 K. Thermogravimetric analysis (TGA) was performed on 2 mg of samples using a Perkin-Elmer thermal analyzer. The samples were heated from 40 to 600 °C at a heating rate of 10.0 °C min^{-1}. A 10 mL min^{-1} flow of dry nitrogen was used to purge the sample all the time. The removal ability of MMS-Py for Hg^{2+} in water was measured using an inductively coupled plasma (ICP) spectrometer (Perkin-Elmer). All spectrophotometic spectra of the hybrid material were performed with a suspension of sample dispersed in deionized water and then brought into a quartz cell for measurement. All photoluminescence (PL) spectra were measured with a Hitachi F-4500 fluorescence spectrophotometer. All spectroscopic measurements were performed in at least triplicate.

3. RESULTS AND DISCUSSION

3.1. Synthesis and characterization of MMS–Py. The synthetic protocol is represented in Scheme 1. As revealed by SEM images, the obtained Fe_3O_4 particles are uniform with a mean diameter of ~200 nm and nearly spherical with rough surfaces (Figure 1a). The surface roughness is attributed to the fact that the particles are formed by packing many nanocrystals. Compared with the magnetite particles, the obtained MMS (Figure 1b) exhibit a more regular spherical shape with smooth surface due to the deposition and growth of silica occurring on a molecular scale caused by the sol–gel process.[13] In the wide-angle XRD pattern of MMS (Figure S2, Supporting Information), the MMS microspheres have diffraction peaks similar to those of the parent Fe_3O_4 particles, proving the well-retained magnetite phase in silica matrix. The presence of core Fe_3O_4 nanoparticles is confirmed by line scanning analysis in the STEM-EDS mode (see Figure S3, Supporting Information). This result reveals that the content of Fe is concentrated in the inner core ranging from 300 to 550 nm and the distribution of silicon across the whole surface is uniform as the shell. Because of the aggregation of Fe_3O_4 nanoparticles prior to the coating process, more than one magnetic nanoparticles (Figure 1c) were trapped in each composite sphere, which is advantageous when manipulating the core–shell nanoparticles with external magnetic force. Furthermore, the mesopore channels are found to be perpendicular to the surface as shown in TEM image (Figure 1d). The unique pore orientation is attributed to the preferred alignment of surfactant/siliceous oligomer composites to the preformed colloidal particles, which may help to significantly decrease the interface energy in the system.[14]

Low-angle XRD patterns of MMS display three resolved diffraction peaks assigned to 100, 110, and 200 reflections of a 2D hexagonal mesostructure (Figure 2 inset up). The N_2 adsorption/desorption isotherm of MMS exhibits type–IV curves (Figure 2) according to IUPAC classification, which further indicates the presence of textual mesopores with a narrow pore size distribution at 2.7 nm (inset down of Figure 2). The BET surface area and total pore volume are calculated to be as high as 676 $m^2 \cdot g^{-1}$ and 0.46 $cm^3 \cdot g^{-1}$, respectively. The uniform mesoporous pore size along with the large surface area and pore volume is advantageous and favorable for the sensing and adsorption of Hg^{2+}.

The fluorescence of MMS-Py (Figure 3) depicts an obvious increase centering at ~462 nm, compared to MMS under the same experimental conditions, which confirms the successful incorporation of receptor Py into the hybrid material. FT-IR spectra of MMS-Py (see Supporting Information, Figure S4) exhibit several new bands at about 1692 cm^{-1} (—C═O stretch

dx.doi.org/10.1021/la204494v | Langmuir 2012, 28, 1657–1662

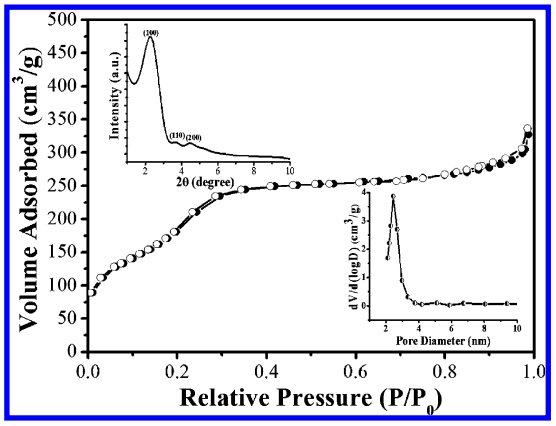

Figure 2. Nitrogen adsorption−desorption isotherms pore size distribution (inset down) of MMS, and the low-angle XRD pattern of the MMS (inset up).

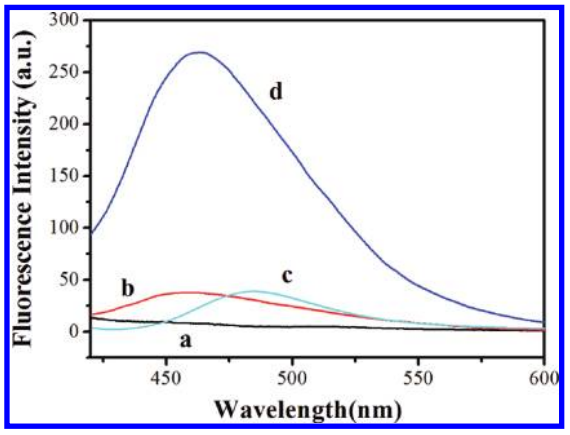

Figure 3. Fluorescence spectra of (a) MMS, (b) MMS−Py, (c) Py−OH, and (d) MMS−Py+Hg^{2+} in aqueous solution. Excitation was at 395 nm, emission was monitored at 462 nm.

I), 1645 cm^{-1} (C—O stretch II), and 1515 cm^{-1} (N—H bend), respectively. The appearance of these new bands also confirms the presence of the fluorescent chromophore Py into the magnetic mesoporous siliia nanocomposites. The content of incorporated receptor Py is determined from TGA measurement. From the TGA results (Figure S5, Supporting Information), it can be calculated that MMS−Py contains approximately 6 wt. % of receptor Py,[16] which means that MMS−Py used in our further solution experiments corresponds to about 0.172 mmol·g^{-1} of receptor Py.

The magnetic measurement on Fe_3O_4 nanoparticles and MMS-Py is shown in Figure 4a. The magnetization saturation values were measured to be 80.7 and 41.5 emu·g^{-1} for Fe_3O_4 nanoparticles and MMS-Py, respectively. Surprisingly, both of them show no hysteresis, which means that they exhibit superparamagnetic behavior at room temperature. According to literature reports,[15] Fe_3O_4 nanoparticles owning diameter larger than ~30 nm have demonstrate coercivity, while, those with smaller diameter have no remanence or coercivity. Considering that the Fe_3O_4 inner core of MMS-Py owns a diameter of ~200 nm, it seems to be unreasonable to observe the superparamagnetic behavior of Fe_3O_4 nanoparticles and MMS-Py. We believe that no remanence or coercivity was detected at room temperature due to the fact that magnetite nanoparticles in the silica spheres are composed of ultrafine magnetite nanocrystals, and this hypothesis can find a clue from Figure

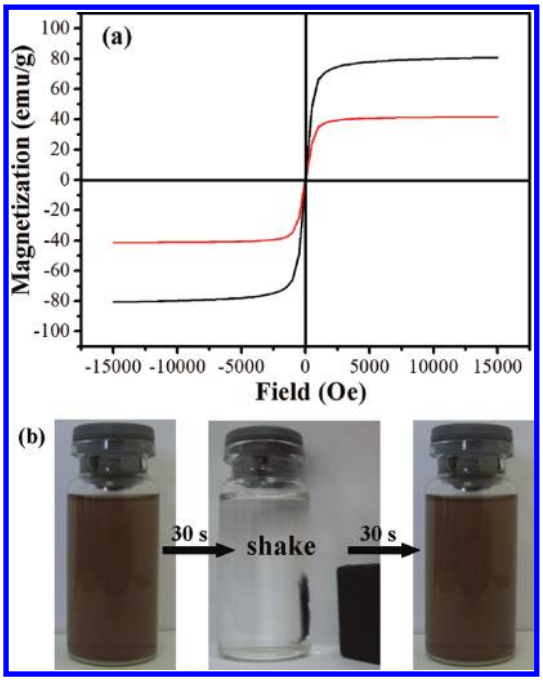

Figure 4. (a) Magnetic hysteresis loops of pure Fe_3O_4 (black line) and MMS−Py (red line), and (b) the separation-redispersion process of MMS−Py.

1A, where tiny particles are found all over the Fe_3O_4 nanoparticles. As a result of the magnetite content, MMS-Py microspheres can quickly respond to external magnetic field and quickly be redispersed homogeneously upon slight shake (Figure 4b). This kind of magnetic property enables MMS-Py to be used for simple and efficient magnetic separation.

3.2. Sensing Performance of the MMS−Py toward Hg^{2+}. The fluorescence emission spectrum of free MMS−Py (20 mg·L^{-1}) displays a broad band peaking at 462 nm (Figure 3), showing a blue shift of about 13 nm compared to that of the Py−OH. Such blue-shift can be interpreted in terms of molecular orbital confinement theory that all energy levels of guest molecules increase in the channel of the host as a result of the confinement.[17] In our hybrid material the increase in energy levels of the Py−OH molecule probably results in the blue shift of MMS−Py spectrum. However, the emission intensity of MMS−Py remains to be constant compared to the Py−OH owing to the thick silica layer. As we know, if a fluorescent dye is attached on the surface of iron oxide nanoparticles, most of the fluorescence should be quenched. But if the dye is far away enough from the core iron oxide, quenching of the fluorescence will be prevented.[18] Therefore, the thick silica layer would be useful not only to serve as the support of fluorescent probes, but also to keep the distance between the core and the surface.

To evaluate the sensing behavior of MMS−Py, its fluorescence in aqueous solution as function of Hg^{2+} concentration is measured. The fluorescence emission spectrum of free MMS−Py in solution shows a weak fluorescence of 462 nm (λ_{ex} = 395 nm), owing to the quenching of pyrene emission by the lone pair of nitrogen atoms in free state.[19] After addition of increasing concentration of Hg^{2+} to the solution, the fluorescence intensity is dramatically enhanced as shown in Figure 5. The fluorescence quenching of pyrene moiety could be ascribed to a photoinduced electron transfer (PET) mechanism, since the emission wavelength is hardly varied during the coordination of Hg^{2+}.[20] So, it could be expected that,

dx.doi.org/10.1021/la204494v | Langmuir 2012, 28, 1657−1662

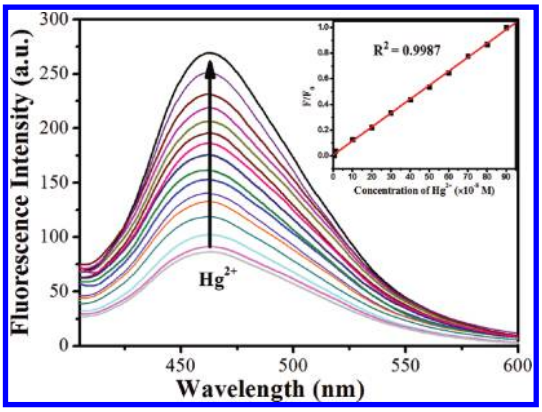

Figure 5. Fluorescence spectra of MMS−Py (20 mg·L^{-1}) upon addition of various amounts of Hg^{2+} in aqueous solution. Inset: emission intensities at 462 nm MMS−Py (20 mg·L^{-1}) as a function of the Hg^{2+} in the lower concentration range (10^{-9}−9× 10^{-7} M). Excitation at 395 nm.

upon complexation with Hg^{2+}, the lone pairs no longer participate in the quenching process, causing the recovery of pyrene fluorescence. A good linearity between I/I_0 and concentration of Hg^{2+} in the range of 10^{-9}−10^{-7} mol·L^{-1} is obtained with a linearly dependent coeffcient R^2 of 0.9987 (Figure 5, inset). The detection limit for Hg^{2+} ion is calculated to be about 1.72 ppb under optimized conditions, which is sufficient to sense the Hg^{2+} concentration in drinking water with respect to U.S. EPA limit (∼2 ppb).[21] This value is found to be 2 orders of magnitude lower than that based on bulk mesoporous materials.[11] The low detection limit relies on the fact that the mesopores on the surface of MMS-Py can efficiently enrich the local Hg^{2+} concentration round Py receptor and thus lead to efficient emission enhancement.

Fluorophores are usually disturbed by proton during detection procedures, so their low sensitivity to operational pH value is highly expected. Consequently, the fluorescence emission intensities of MMS-Py with and without Hg^{2+} as a function of pH are shown in Figure 6. The suitable range of pH

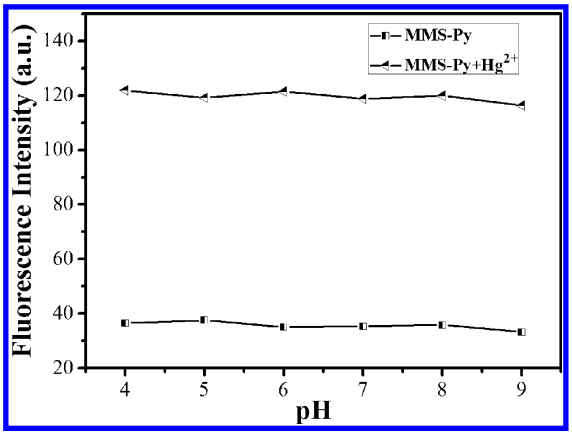

Figure 6. Variation of fluorescence intensity at 462 nm of MMS−Py (20 mg·L^{-1}) in aqueous solution with and without 10^{-6} M Hg^{2+} as a function of pH. Excitation at 395 nm.

for Hg^{2+} determination is found to be between pH 4.0 and 9.0, suggesting that no buffer solutions are required for the detection of Hg^{2+}, and MMS-Py is suitable and qualified enough for practical applications.

An highly desired feature of the Hg^{2+} sensing material is the selectivity toward Hg^{2+} ions over competitive ionic species, such as Zn^{2+}, Cu^{2+}, Cd^{2+}, Pb^{2+}, Co^{2+}, Ag^{+}, Mg^{2+}, Ca^{2+}, Fe^{3+}, and Na^{+}. To get a view on the selectivity of MMS−Py, the fluorescence spectra are recorded at 462 nm within 2 min from the addition of these metal ions (at 10^{-3} M) to a suspension of MMS−Py (20 mg·L^{-1}). Figure 7 illustrates the fluorescence

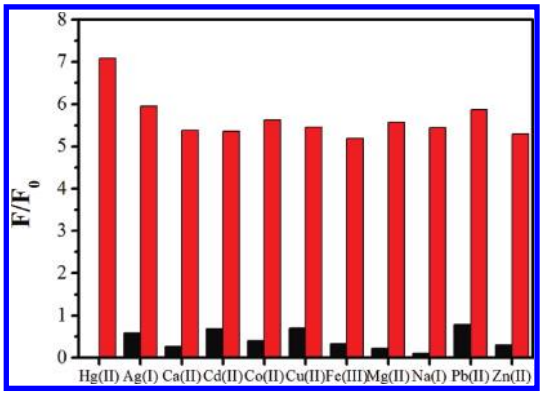

Figure 7. Normalized fluorescence responses of MMS−Py (20 mg·L^{-1}) to various cations in aqueous solution. The black bars represent the emission intensities of MMS−Py in the presence of various interfering ions (all at 10^{-3} M). The red bars represent the change of the emission that occurs upon the subsequent addition of 10^{-6} M of Hg^{2+} to the above solution. The intensities were recorded at 462 nm, excitation at 395 nm.

responses of MMS−Py to various metal ions and its selectivity toward Hg^{2+} over these metal ions. No significant spectral changes of the suspension solution are observed in the presence of these metal ions. Only the addition of Hg^{2+} (10^{-6} M) ions into the suspension of MMS−Py produces a dramatic increasing in fluorescence intensity, revealing that Hg^{2+}-specfic responses is not disturbed by the competitive ions.

3.3. Regeneration and Removal Abilities of MMS−Py.

The regeneration ability of MMS−Py after immersion in Hg^{2+} (10^{-6} M) is examined. After being immersed in Hg^{2+} solution, the fluorescence change of MMS−Py was found to be fully recovered upon rinsing with 100 mM of EDTA (sodium salt). Reusability is evaluated by repeated immersing/rinsing cycles, with the fluorescence spectrum being recorded after each step. Results are shown in Figure 8. The fluorescence changes are reproducible over several cycles. It is apparent that the MMS−Py exhibits excellent reusability since almost no loss in MMS−Py sensitivity is observed after 8 repeated immersing/rinsing cycles. Furthermore, the rapid response time of the system, with the fluorescent change being complete within a few seconds, allows the potential for rapid recovery of sensing function. The results clearly indicate that MMS−Py is stable under these operating conditions and demonstrates its excellent recyclability.

The removal ability of MMS−Py in solid−liquid phase is also estimated in order to evaluate its potential as a practical absorbent material for Hg^{2+}. A Hg^{2+} solution of about 3 × 10^{-6} M (1 ppm; 50 mL) is treated with 20 mg of MMS−Py for a few cycles, after filtration, the concentration of residual Hg^{2+} in the filtrate is analyzed by ICP source mass spectrometer. Interestingly, no residual levels of Hg^{2+} is detectable in the filtrate after three cycles, suggesting that the designed MMS−Py can remove Hg^{2+} from aqueous solutions completely and efficiently.

dx.doi.org/10.1021/la204494v | Langmuir 2012, 28, 1657−1662

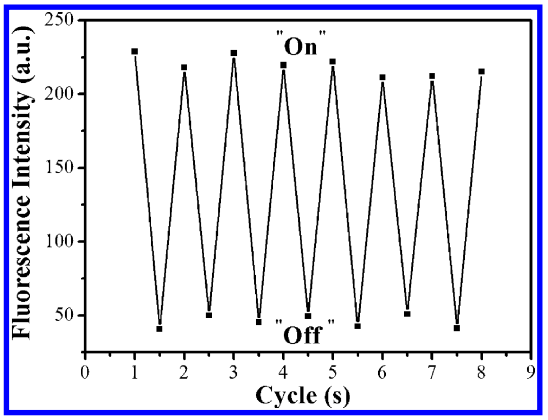

Figure 8. Fluorescence responses of MMS−Py (20 mg·L^{-1}) by alternated dipping in 10^{-6} M aqueous solution of Hg^{2+} ("ON") and 100 mM of EDTA (sodium salt) ("OFF"). The cyclic index is the number of alternating immersing/rinsing cycles.

4. CONCLUSION

In conclusion, a novel functionalized magnetic mesoporous nanomaterial is designed and constructed by covalent coupling of the pyrene-based receptor Py within the channels of magnetic mesoporous silica nanocomposites. In comparison to the bulk meoporous material, the fluorescent sensing properties of Py receptor in our nanostructure are significantly improved. MMS-Py recognizes Hg^{2+} with a high selectivity and sensitive fluorescence response in aqueous solution with detection limit as low as 1.72 ppb. The fluorogenical responses are reversible and stable over a broad (4.0−9.0) pH range, suitable for application under physiological conditions. Moreover, MMS-Py can be used as a reusable absorbent for fast, convenient, and highly efficient removal of Hg^{2+}. We believe that the combination of well-defined inorganic nanomaterials and organic receptors can play a vital role in the development of a new generation of toxic metal ions chemosensor and absorbent.

■ ASSOCIATED CONTENT

Supporting Information

FT-IR spectra of as-synthesized MMS, surfactant-extracted MMS, MMS−Py, and Py, the wide-angle XRD patterns of Fe_3O_4 and MMS, STEM images of the MMS microspheres, and TGA analysis of MMS-Py. This material is available free of charge via the Internet at http://pubs.acs.org.

■ AUTHOR INFORMATION

Corresponding Author

*Tel/fax: +86 431 86176935. E-mail: lib020@yahoo.cn.

■ ACKNOWLEDGMENTS

The authors gratefully thank the financial supports of the NSFC (Grant Nos. 51172224 and 51103145) and the Science and Technology Developing Project of Jilin Province (Grant No. 20100533).

■ REFERENCES

(1) (a) Quirarte-Escalante, C. A.; Soto, V.; de la Cruz, W.; Porras, G. R.; Manríquez, R.; Gomez-Salazar, S. *Chem. Mater.* **2009**, *21*, 1439−1450. (b) Yang, Y. Y.; Cheng, T. Y.; Zhu, W. P.; Xu, Y. F.; Qian, X. H. *Org. Lett.* **2010**, *13*, 264−267. (c) Wang, H. G.; Sun, L.; Li, Y. P.; Fei, X. L.; Sun, M. D.; Zhang, C. Q.; Li, Y. X.; Yang, Q. B. *Langmuir* **2011**, *27*, 11609−11615. (d) Cheng, T. Y.; Xu, Y. F.; Zhang, S. Y.; Zhu, W. P.; Qian, X. H.; Duan, L. P. *J. Am. Chem. Soc.* **2008**, *130*, 16160−16161. (e) Meng, Q. T.; Zhang, X. L.; He, C.; He, G. J.; Zhou, P.; Duan, C. Y. *Adv. Funct. Mater.* **2010**, *20*, 1903−1909. (f) Park, M.; Seo, S.; Lee, I. S.; Jung, J. H. *Chem. Commun.* **2010**, *46*, 4478−4480. (g) Zhang, X. L.; Xiao, Y.; Qian, X. H. *Angew. Chem., Int. Ed.* **2008**, *47*, 8025−8029.

(2) (a) von Burg, R. *J. Appl. Toxicol.* **1995**, *15*, 483−493. (b) Harris, H. H.; Pickering, I. J.; George, G. N. *Science* **2003**, *301*, 1203.

(3) (a) Castanotto, D.; Rossi, J. J. *Nature* **2009**, *457*, 426−433. (b) Deng, Y. H.; Deng, C. H.; Qi, D. W.; Liu, C.; Liu, J.; Zhang, X. M.; Zhao, D. Y. *Adv. Mater.* **2009**, *21*, 1377−1382. (c) Bouffier, L.; Yiu, H. H. P.; Rosseinsky, M. J. *Langmuir* **2011**, *27*, 6185−6192.

(4) (a) Feng, J.; Song, S. Y.; Deng, R. P.; Fan, W. Q.; Zhang, H. J. *Langmuir* **2010**, *26*, 3596−3660. (b) Erogbogbo, F.; Yong, K.-T.; Hu, R.; Law, W.-C.; Ding, H.; Chang, C.-W.; Prasad, P. N.; Swihart, M. T. *ACS Nano* **2010**, *4*, 5131−5138.

(5) (a) Xu, X.; Deng, C.; Gao, M.; Yu, W.; Yang, P.; Zhang, X. *Adv. Mater.* **2006**, *18*, 3289−3293. (b) Goon, I. Y.; Zhang, C.; Lim, M.; Gooding, J. J.; Amal, R. *Langmuir* **2010**, *26*, 12247−12252.

(6) (a) Deng, Y. H.; Cai, Y.; Sun, Z. K.; Liu, J.; Liu, C.; Wei, J.; Li, W.; Liu, C.; Wang, Y.; Zhao, D. Y. *J. Am. Chem. Soc.* **2010**, *132*, 8466−8473. Xuan, S.; Wang, Y.-X. J.; Yu, J. C.; Leung, K. C.-F. *Langmuir* **2009**, *25*, 11835−11843.

(7) (a) Han, W. S.; Lee, H. Y.; Jung, S. H.; Lee, S. J.; Jung, J. H. *Chem. Soc. Rev.* **2009**, *38*, 1904−1915. (b) Descalzo, A. B.; Martínez-Máñez, R.; Sancenón, F.; Hoffmann, K.; Rurack, K. *Angew. Chem., Int. Ed.* **2006**, *45*, 5924−5948.

(8) Melde, B.; Johnson, B. *Anal. Bioanal. Chem.* **2010**, *398*, 1565−1573.

(9) Martínez-Máñez, R.; Sancenón, F.; Hecht, M.; Biyikal, M.; Rurack, K. *Anal. Bioanal. Chem.* **2011**, *399*, 55−74.

(10) (a) Wang, C.; Tao, S. Y.; Wei, W.; Meng, C. G.; Liu, F. Y.; Han, M. *J. Mater. Chem.* **2010**, *20*, 4635−4641. (b) Ros-Lis, J. V.; Casasús, R.; Comes, M.; Coll, C.; Marcos, M. D.; Martínez-Máñez, R.; Sancenón, F.; Soto, J.; Amorós, P.; Haskouri, J. E.; Garró, N.; Rurack, K. *Chem.—Eur. J.* **2008**, *14*, 8267−8278. (c) Lee, S. J.; Lee, J. E.; Seo, J.; Jeong, I. Y.; Lee, S. S.; Jung, J. H. *Adv. Funct. Mater.* **2007**, *17*, 3441−3446.

(11) Wang, Y. H.; Li, B.; Zhang, L. M.; Liu, L. N.; Zuo, Q. H.; Li, P. *New J. Chem.* **2010**, *34*, 1946−1953.

(12) Deng, Y. H.; Qi, D. W.; Deng, C. H.; Zhang, X. M.; Zhao, D. Y. *J. Am. Chem. Soc.* **2007**, *130*, 28−29.

(13) Stöber, W.; Fink, A.; Bohn, E. *J. Colloid Interface Sci.* **1968**, *26*, 62−69.

(14) (a) Tan, B.; Rankin, S. E. *J. Phys. Chem. B* **2004**, *108*, 20122−20129. (b) Yoon, S. B.; Kim, J.-Y.; Kim, J. H.; Park, Y. J.; Yoon, K. R.; Park, S.-K.; Yu, J.-S. *J. Mater. Chem.* **2007**, *17*, 1758−1761.

(15) (a) Deng, Y. H.; Wang, C. C.; Shen, X. Z.; Yang, W. L.; Jin, L.; Gao, H.; Fu, S. K. *Chem.—Eur. J.* **2005**, *11*, 6006−6013. (b) Ge, J. P.; Hu, Y. X.; Biasini, M.; Beyermann, W. P.; Yin, Y. D. *Angew. Chem., Int. Ed.* **2007**, *46*, 4342−4345. (c) Stjerndahl, M.; Andersson, M.; Hall, H. E.; Pajerowski, D. M.; Meisel, M. W.; Duran, R. S. *Langmuir* **2008**, *24*, 3532−3536. (d) Wang, Y. L.; Xu, H.; Ma, Y. S.; Guo, F. F.; Wang, F.; Shi, D. L. *Langmuir* **2011**, *27*, 7207−7212.

(16) Tien, P.; Chau, L.-K. *Chem. Mater.* **1999**, *11*, 2141−2147.

(17) (a) Zhang, L. Z.; Xiong, Y.; Cheng, P.; Tang, G. Q.; Liao, D. Z. *Chem. Phys. Lett.* **2002**, *358*, 278−283. (b) Zhang, L.; Sun, W.; Cheng, P. *Molecules* **2003**, *8*, 207−222.

(18) Weissleder, R.; Kelly, K.; Sun, E. Y.; Shtatland, T.; Josephson, L. *Nat. Biotechnol.* **2005**, *23*, 1418−1423.

(19) Davidson, R. S. In *Adv. Phys. Org. Chem.*, Vol. *19*; Gold, V., Bethell, D., Ed.; Academic Press, 1983; pp 1−130.

(20) de Silva, A. P.; Gunaratne, H. Q. N.; Gunnlaugsson, T.; Huxley, A. J. M.; McCoy, C. P.; Rademacher, J. T.; Rice, T. E. *Chem. Rev.* **1997**, *97*, 1515−1566.

(21) *Mercury Update: Impact on Fish Advisories*; EPA Fact Sheet EPA-823-F-01-011; EPA, Office of Water: Washington, DC, 2001.